

Evaluation of Unionized Propellant Xenon Atom in a Hall Thruster Plume

Makoto Matsui^a, Shigeru Yokota^a, Kimiya Komurasaki^b and Yoshihiro Arakawa^a

^a*Department of Aeronautics and Astronautics, University of Tokyo, 7-3-1 Hongo, Bunkyo, Tokyo 113-8656, Japan*

^b*Department of Advanced Energy, University of Tokyo, 5-1-5 Kashiwanoha, Kashiwa, Chiba 277-8561, Japan*

Abstract. Unionized propellant xenon atom in a magnetic layer type Hall thruster plume was diagnosed by optical methods. To estimate the total xenon number density from previously measured meta-stable one, the Boltzmann, the corona and the KCD models were evaluated by emission spectroscopy. The measured xenon spectra show better agreement with the KCD model than the others. Also the electron temperature by a combination of the KCD model with the measured spectra shows good agreement with that from a single probe measurement. As a result of the application of this model, the total number density of xenon was estimated $3.4 \times 10^{19} \text{ m}^{-3}$ at the channel exit and decreased by $1/e$ at 60 mm from the exit.

Keywords: Hall thruster, Plasma physics, Non-equilibrium flow, Plasma spectroscopy.

PACS: 94.20.Fg, 47.70.Nd, 47.45.-n.

INTRODUCTION

Hall thrusters are one of the promising thrusters of satellites for orbit transfer or North/South station keeping missions because it produces high thrust efficiency, exceeding 50%, with a specific impulse range of 1000-3000 s and a higher ion beam density than ion thrusters because of the existence of electrons in the ion acceleration zone. This is because a moderate magnetic field is applied in the acceleration zone, causing the magnetization of the electrons and not the ions. Hence, several types of Hall thrusters are actively developed in Russia, USA, EU and Japan [1-3].

In their practical use in a spacecraft, the interactions between the plume of the thruster and the host spacecraft cause serious problems [4,5]. High-energy main beam ions generated and accelerated in the acceleration channel collide with unionized propellant atoms in the plume, resulting in the production of low-energy ions and high-energy atoms by charge exchange reaction (CEX). These CEX ions propagate in the radial and upstream directions because of the potential distribution near the spacecraft. The backflow of CEX ions becomes a contamination source causing erosion, sputtering, degradation, increment of temperature and potential change of solar arrays or spacecraft surfaces.

Recently, a plume shield has been developed to protect the spacecraft from CEX ions. The plume shield developed by Mitsubishi Electric Corporation intercepts ions with higher angle beyond 45 degree [6]. Then, it is important to clarify a production mechanism of CEX reactions to evaluate the shield's performances and optimization. Plume characteristics have been a hot subject and investigated experimentally in ground-based facilities [7,8] and even in an actual flight test [9] as well as numerical calculations [10,11]. Because most of measurements, however, are conducted by intrusive probe methods such as electrostatic probes, energy analyzers and mass spectrometers, measurements near the thruster exit are difficult for their disturbances, where CEX reactions would most frequently take place. The plume properties near the thruster exit are also useful for initial conditions of numerical calculations.

In our previous research, laser absorption spectroscopy (LAS) and single probe measurements were applied to a magnetic-layer-type hall thruster plume developed at the University of Tokyo [12-14]. The number density distributions of meta-stable xenon atom ($1s_5$) were measured in two different ambient pressure conditions to evaluate the influence of the background xenon on the measurement. Then the number density distribution of the

propellant meta-stable xenon atom (1s5) was estimated separately from the background one as shown in Fig.1. However, in a hall thruster plume, electronic excitation states do not obey Boltzmann distribution due to the low ambient pressure of 10^{-3} Pa [15]. Then, the relationships between meta-stable and other states including ground state are necessary to obtain total number density distribution. In this study, a collisional-radiative model developed by Karabadzahk et.al. [16,17] and recent collision cross section data by Jung et.al. [18] were applied to deduce the total number density. Then, the model was evaluated by emission spectroscopy.

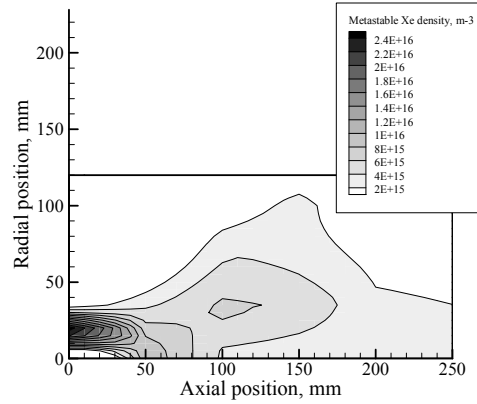


FIGURE 1. Number density distribution of meta-stable xenon (1s5) by laser absorption spectroscopy.

COLLISIONAL RADIATIVE MODEL

Boltzmann Model

In a local thermo-equilibrium plasma, the internal states obey Boltzmann distributions. In this case, the emission intensity $J_{\lambda}^{\text{Boltzmann}}(\text{XeI})$ is expressed as,

$$J_{\lambda}^{\text{Boltzmann}}(\text{XeI}) \propto \frac{A_{21}g_2}{\lambda} \exp\left(-\frac{E_2}{k_B T_e}\right) \quad (1)$$

Here, A , g , λ , E , k_B and T_e are the Einstein coefficient¹⁹, statistical weight, wavelength, excitation energy, Boltzmann constant and electron temperature, respectively.

Assuming the total number density N_0 is nearly equal to the ground state number density N_g , it is related to the meta-stable number density N_m expressed as,

$$N_0 \sim N_g = N_m \frac{g_g}{g_m} \exp\left(\frac{E_m}{k_B T_e}\right) \quad (2)$$

KCD Model

Although many researchers have applied corona model to hall thruster plumes, Karabadzahk et.al. have developed a more precise collisional radiative model of xenon atom (KCD model). They consider nine xenon atomic states tabulated in Table 1 and based on the corona model, they have added to the electron collision with meta-stable xenon atom and the ion xenon collision with xenon atom. As a result, the emission intensity is expressed as,

$$J_{\lambda}^{\text{KCD}}(\text{XeI}) \propto \frac{1}{\lambda} (k_{e0}^{\lambda} + \alpha k_1^{\lambda} + \frac{1-\alpha}{2} k_2^{\lambda}) \left[1 + \frac{K^{\lambda}(T_e, \alpha)}{\zeta^{\lambda}} \right] \quad (3)$$

Here, α is the ratio of the first ion number density to the electron number density, k_{e0}^{λ} , k_1^{λ} , k_2^{λ} are the emission excitation rate coefficient for electron collisions with ground state xenon atom, for collisions of Xe^+ and Xe^{2+} with neutral xenon atoms, respectively. $K^{\lambda}(T_e, \alpha)$ is defined as,

$$K^{\lambda}(T_e, \alpha) = \frac{\sum_i \{k_{e0}^i + \alpha k_1^i + [(1-\alpha)/2] k_2^i\}}{k_{e0}^{\lambda} + \alpha k_1^{\lambda} + [(1-\alpha)/2] k_2^{\lambda}} \quad (4)$$

Here, the sum in the numerator is the coupled lines with meta-stable $K^{\lambda}(T_e, \alpha)$ is zero for uncoupled lines with meta-stable. ζ^{λ} is the calculated parameter depending on the emission excitation rate coefficient for electron collisions with meta-stable xenon atom and branching factor as tabulated in Table 1.

It is remarked that when k_1^{λ} , k_2^{λ} and $K^{\lambda}(T_e, \alpha)$ are set to zero, Eq.(1) is identical to the emission intensity by the corona model.

The total number density N_0 is related to the meta-stable one N_m , expressed as

$$N_0 = N_m \frac{\sum_i P_{ri} T_i}{\sum_i \{k_{e0}^i + \alpha k_1^i + [(1-\alpha)/2] k_2^i\}} \quad (5)$$

Here, the sum in the numerator is the same as in Eq.(2) and P_{ri} are the branching coefficients for a relative transition from the upper $2p_i$ state into $1s_4$ state. T_i are the excitation rate coefficients from meta-stable to upper states and unknown parameter in KCD model. Here, we calculated T_i using the electron impact excitation cross section by Jung et.al. assuming the electron energy distribution function is the Maxwell one. Figure 2 shows the calculated T_i .

TABLE 1. Excitation states used in KCD model and parameters.

	$2p_1 \rightarrow 1s_4$	$2p_3 \rightarrow 1s_4$	$2p_5 \rightarrow 1s_4$	$2p_6 \rightarrow 1s_5$	$2p_7 \rightarrow 1s_5$	$2p_7 \rightarrow 1s_4$	$2p_8 \rightarrow 1s_5$	$2p_9 \rightarrow 1s_5$	$2p_{10} \rightarrow 1s_5$
λ , nm	788.7	834.7	828.0	823.2	840.9	916.3	881.9	904.5	980.0
E_{2p_i} , eV	11.14	11.05	9.93	9.82	9.79	9.79	9.72	9.69	9.58
g_{2p_i}	1	5	1	5	3	3	7	5	3
ζ^{λ}				1.89	23.96	2.632	1.016	3.754	2.430
$1-P_{ri}$				0.753	0.099	(0.901)	1.0	0.379	0.976

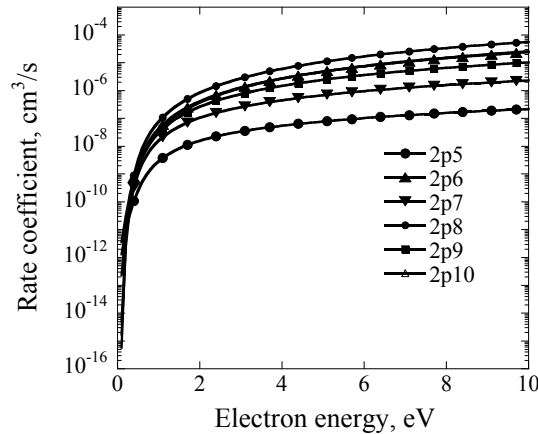


FIGURE 2. Excitation rate coefficient for electron collisions with meta-stable xenon atom.

EXPERIMENTAL SETUP

Magnetic Layer Type Hall Thruster

Figures 3 and 4 show a cross section of a magnetic-layer-type Hall thruster and its photo in operation. The inner and outer diameters of the acceleration channel are 48 and 62 mm, respectively. An acceleration channel wall was made of BN. The anode is located at 21 mm, upstream end of the acceleration channel. A solenoid coil is set at the center of the thruster to apply a radial magnetic field in the acceleration channel. The magnetic flux density is varied by changing the coil current. There is no outer coil because a uniform magnetic field distribution is maintained along the azimuthal direction. A hollow cathode (7HCN-001-001; Veeco-Ion Tech Inc.) was used as an electron source and a neutralizer. A vacuum chamber of 2 m diameter by 3 m length was used in the experiments. The pumping system comprised a diffusion pump (37000 l/s), a mechanical booster pump (2800 l/s), and two rotary pumps (250 l/s). Two operation conditions are tabulated in Table 2.

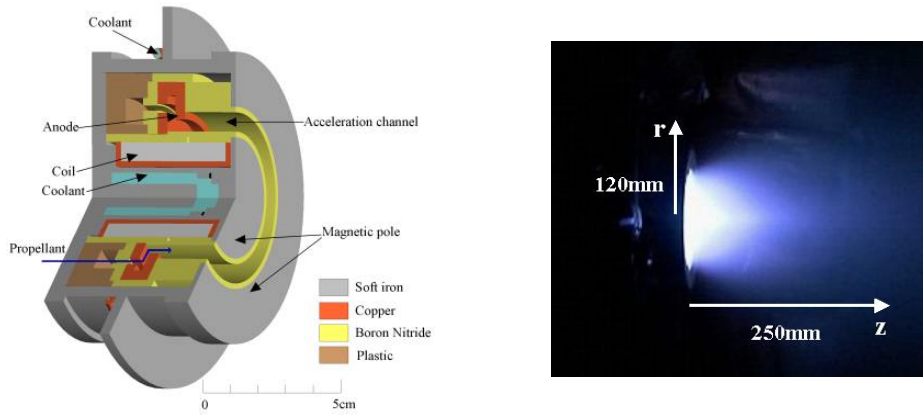


FIGURE 3. Cross sectional view of UT magnetic layer type Hall thruster (left) and its plume photo (right).

TABLE 2. Operation conditions.

Parameters	Values
Propellant gas	Xe: 1.0Aeq (1.36 mg/s)
Discharge voltage	260 V
Discharge current	1.2 A
Applied magnetic field	11.2 mT
Ambient pressure	2.77×10^{-3} a

Emission Spectroscopy

Emission spectra collected by collimate lens (FC230-B, Thorlab Inc.) with an optical fiber whose core diameter was 400 μm were measured by a multi-channel spectrometer (HR4000, Ocean Optics Inc.). This spectrometer can detect the spectra in the range of 200 nm to 1100 nm with the wavelength resolution of 0.49 nm at a time. The sensitivity was calibrated by standard light source (OL245C, Optronic Laboratories, Inc.). The exposure time was set to 600 ms. The collimator lens was mounted two dimensional traverse stage and the spectra were measured at every 10 mm in the radial direction and 50 mm in the axial direction.

Since the detected spectra were parallel integrated values, the Abel inversion [20] was applied to obtain the radial spectra by the following equation.

$$J(r) = \frac{1}{\pi} \int_r^R \frac{d(J(y))}{dy} \frac{dy}{\sqrt{y^2 - r^2}} \quad (6)$$

Here, y is the lens position and R is the plume radius.

RESULTS AND DISCUSSION

Figure 4 shows measured and calculated line intensities normalized by 881.9 nm line at $r=20$ mm. In the models, the electron temperature was varied as a fitting parameter. The line intensities in the KCD model show better agreement with the experimental result than corona and Boltzmann models. However, there are some discrepancies for the 823.2 nm, 904.5 nm and 916.3 nm lines. Since these lines are related with the meta-stable, these discrepancies might be because of the uncertainty of the rate coefficient from the meta-stable to higher levels. The other reason is the intensity analysis. Although in this study peak values were used as the line intensities, the profile area is more accurate especially for the channel exit region, where the line is broadened by the Zeeman splitting.

The electron temperature distributions estimated by the KCD model are also plotted in Figure 4 along with that in the previous single probe measurement [13]. The electron temperature by the model has a peak value of 7.9 eV at $z=0$ mm then decreases gradually. This result shows good agreement with the probe one.

Figure 5 shows number density distributions of estimated total xenon atom and measured meta-stable at $r=20$ mm, which is the line parallel to the axis at the channel exit. The total number density of xenon by the KCD model was $3.4 \times 10^{19} \text{ m}^{-3}$ at the channel exit and decreased by $1/e$ at 60 mm from the exit. This value is reasonable because the number density estimated from the mass flow rate, the thermal velocity and the propellant utilization efficiency of 0.8 and channel exit area of 12.1 cm^2 is $1.2 \times 10^{19} \text{ m}^{-3}$ at the channel exit. On the other hand, in the Boltzmann model, the estimated number density is of the same order as the meta-stable one, which means extremely high propellant utilization efficiency. Then, the meta-stable does not have the Boltzmann relation with the ground state.

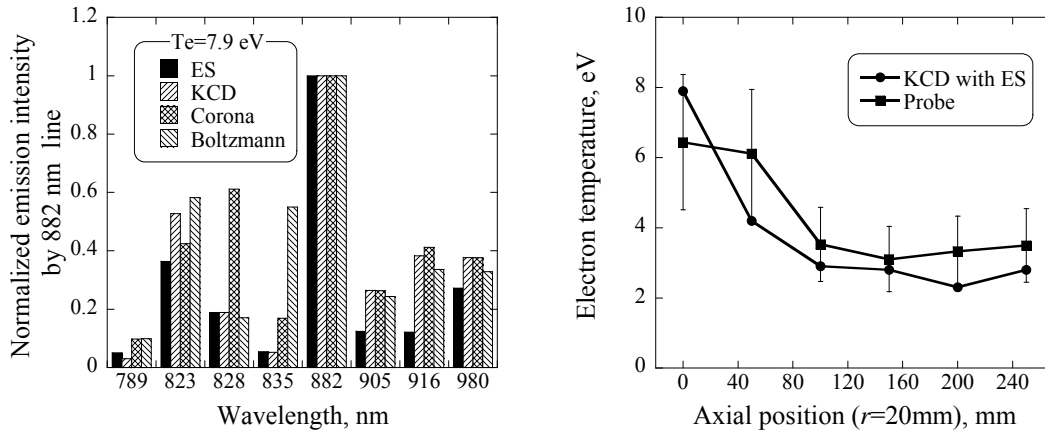


FIGURE 4. Models evaluation; relative line intensity normalized by 881.9 nm line by the experiment, KCD, corona and Boltzmann models (left) and electron temperature distributions by KCD model and single probe measurement (right).

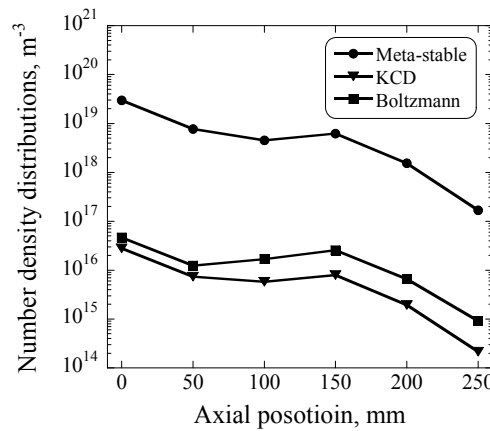


FIGURE 5. Estimated total number density distributions of xenon atom, $r=30$ mm.

CONCLUSION

Excitation rate coefficients from meta-stable to upper states were calculated using the cross section data by Jung et.al. assuming Maxwell distribution of the electron energy. Then, they were built into the collisional-radiative model developed by Karabadzahk et.al. This model was coupled with the emission spectroscopy. The measured atomic spectra show better agreement with the model than conventional Boltzmann and corona models. The electron temperature estimated from the model and the emission lines shows good agreement with that in the previous single probe measurement. Finally, the number density distribution of total xenon atom was estimated from the measured meta-stable density by previous laser absorption spectroscopy measurement and the KCD model. The total number density of xenon was $3.4 \times 10^{19} \text{ m}^{-3}$ at the channel exit and decreased by 1/e at 60 mm from the exit.

ACKNOWLEDGMENTS

This work was partially supported by a Grand-in-Aid for Scientific Research (S), No.16106012 and for Research Fellowships of the Japan Society for the Promotion of Science for Young Scientists, 18-09885, 2006 sponsored by the Ministry of Education, Culture, Sports, Science and Technology in Japan.

REFERENCES

1. H. R. Kaufman, *AIAA J.* **23**, 78-86 (1985).
2. E. Y. Choueiri, *Phys Plasmas* **8**, 5025-5033 (2001).
3. N. Yamamoto, K. Komurasaki and Y. Arakawa, *J Propul Power* **21**, 870-876 (2005).
4. I. D. Boyd, *J Spacecraft Rockets* **38**, 381-387 (2001).
5. M. Tajmar, J. Gonzalez and A. Hilgers, *J Spacecraft Rockets* **38**, 393-399 (2001).
6. T. Ozaki, Y. Inanaga, T. Nakagawa, Y. Kasai and K. Matsui, Proceedings of ISTS b-34 (2006).
7. A. D. Gallimore, *J Spacecraft Rockets* **38**, 441-453 (2001).
8. L. B. King and A. D. Gallimore, *J Propul Power* **20**, 228-242 (2004).
9. J. Gonzalez and D. Estublier, *Proceedings of IEPC*, 003, (2005).
10. F. Taccogna, S. Longo and M. Capitelli, *J Spacecraft Rockets* **39**, 409-419 (2002).
11. I. D. Boyd, D. B. Van Gilder and X. Liu, *J Propul Power* **14**, 1009-1015 (1998).
12. M. Matsui, S. Yokota, D. Sakoh, K. Komurasaki and Y. Arakawa, *Proceedings of IEPC*, 46 (2007).
13. Y. Yokota, M. Matsui, D. Sako, N. Nagao, H. Takayanagi, H. Koizumi, K. Komurasaki and Y. Arakawa, *AIAA Paper*, 06-5028 (2006).
14. S. Yokota, D. Sakoh, M. Matsui, K. Komurasaki and Y. Arakawa, *Vacuum* **83**, 57-60 (2008).
15. H. R. Griem, H. R., *Plasma Spectroscopy*, New York: McGraw-Hill, Inc., 1964.
16. Y. Chiu, B. L. Austin, S. Williams, R. A. Dressler and G. F. Karabadzahk, *J Phys* **99**, 113304 (2006).
17. G. F. Karabadzahk, Y. Chiu and R. A. Dressler, *J Phys* **99**, 113305 (2006).
18. R. O. Jung, J. B. Boffard, L. W. Anderson and C. C. Lin, *Phys Rev A* **72**, 022723 (2005).
19. NIST Atomic Spectra Database: http://physics.nist.gov/cgi-bin/AtData/main_asd.
20. M. Deutch, *Appl Phys Letters* **42**, 237-239 (1983).